*American Mineralogist, Volume 108, pages 1708–1719, 2023*

# Mechanism and kinetics of the pseudomorphic replacement of anhydrite by calcium phosphate phases at hydrothermal conditions

**Ana Roza-Llera[1], Amalia Jiménez[1,*], and Lurdes Fernández-Díaz[2]**

[1]Department of Geology, University of Oviedo, 33005 Oviedo Spain
[2]Departmento Cristalografía y Mineralogía, Universidad Complutense de Madrid, José Antonio Novais, 2, E-28040 Madrid, Spain

## Abstract

Mineral replacement reactions mediated by fluids are common in sedimentary basins, where they influence geochemical cycles. Phosphorous (P) pollution of soils, sediments and water bodies is currently a widespread problem. Some apatite accumulations in sediments may have formed through the interaction of P-bearing aqueous solutions with mineral surfaces that result in mineral replacement reactions. Here, we investigate the pseudomorphic replacement of anhydrite single crystals by aggregates of β-tricalcium phosphate and hydroxyapatite upon interaction with a P-bearing solution at temperatures between 120 and 200 °C. SEM imaging is used to study the texture of the aggregates. Rietveld refinement of the X-ray diffraction patterns and Raman spectra analysis of the reacted samples provide information on the kinetics of the replacement. At all temperatures β-tricalcium phosphate forms alongside hydroxyapatite at early stages of the replacement reaction. At $T \geq 180$ °C, hydroxyapatite/β-tricalcium phosphate ratio rapidly increases, and hydroxyapatite is the only phase in fully replaced samples. At $T < 180$ °C hydroxyapatite/β-tricalcium phosphate ratio increases slowly and fully replaced samples still contain significant amounts of β-tricalcium phosphate. The progress of the replacement is facilitated by the formation of porosity. The evolution of the hydroxyapatite/β-tricalcium phosphate ratio and the crystal habit of both phases strongly influence the arrangement of this porosity. The empirical activation energy $E_a$ (kJ/mol) of the replacement reaction is determined by the Avrami and the iso-conversion methods. Both approaches yield an $E_a$ of ~40 kJ/mol. Anhydrite dissolution appears as the rate-limiting process and the overall kinetics of the replacement reaction is controlled by the rate diffusion of dissolved species through the porosity network. The ripening of the metastable β-tricalcium phosphate into hydroxyapatite affects the characteristics of the porosity network and further modulates the kinetics of the replacement. These results may improve the understanding of the mechanisms of P-sequestration by mineral surfaces through coupled dissolution–precipitation reactions and shed light on the origin of apatite accumulations associated to evaporitic sedimentary rocks.

**Keywords:** Anhydrite, hydroxyapatite, β-tricalcium phosphate, mineral replacement, pseudomorphism, kinetics, textures, coupled dissolution-precipitation

## Introduction

Mineral replacements are common processes in sedimentary, diagenetic, metamorphic, and metasomatic environments, where they take place mediated by a fluid that facilitates the dissolution of the primary mineral and the concomitant precipitation of the secondary one(s). The coupling through the interface of the dissolution and precipitation rates allows for the preservation of original shape and volume of the primary mineral (Putnis 2002, 2009; Putnis and Putnis 2007; Pollok et al. 2011; Ruiz-Agudo et al. 2014). Moreover, when the dissolution of the latter is the rate-limiting step of the interface coupled dissolution-precipitation reaction (ICDP), original microscopic, and even nanoscopic, features also are accurately preserved during the replacement (Xia et al. 2009; Ruiz-Agudo et al. 2014; Altree-Williams et al. 2015). The progress of ICDP reactions requires a continuous communication between the interface, where the reaction takes place, and the bulk fluid. This communication is ensured by the formation of a network of porosity and/or fractures during the mineral replacement. This network facilitates mass transport to and from the interfacial fluid (Zhao et al. 2009; Jonas et al. 2013; Ruiz-Agudo et al. 2014; Putnis 2015).

In this work we describe the replacement of anhydrite by mixtures of two calcium phosphate phases, β-tricalcium phosphate [β-$Ca_3(PO_4)_2$] (β-TCP) and hydroxyapatite [$Ca_5(PO_4)_3(OH)$] (Hap) through a ICDP mediated by an aqueous fluid containing phosphorous (P). Anhydrite is a rock-forming mineral common in sedimentary basins, where it appears as a major component of evaporites as well as forming nodules and cements in sandstones, limestones, and dolostones (Murray 1964; Rahimpour-Bonab et al. 2010; Olivarius et al. 2015). Anhydrite also forms massive accumulations in modern submarine hydrothermal vents (Kuhn et al. 2003). Apatite [$Ca_5(PO_4)_3(OH,Cl,F)$] is the main source of phosphorous, an element that is scarce in the Earth's crust but has great economic interest in the fertilizer industry (Filippelli 2002). Phosphorous is an essential macronutrient for biota as well as a pollutant which in excess causes eutrophication of water bodies, contributes to the growth of toxigenic algae, and boosts the development of potentially pathogenic microbes in the water column and in soils (Mallin and Cahoon 2020). The structural

* E-mail: amjimenez@uniovi.es


0003-004X/23/0009–1708$05.00/DOI: https://doi.org/10.2138/am-2022-8592

characteristics of apatite make it a relevant phase for immobilizing and storing of radioactive and other pollutant elements (Rakovan and Reeder 1996; Ewing and Wang 2002; Mavropoulos et al. 2002).

There is abundant evidence that mineral replacement reactions play an important role in controlling the fate of various pollutants in soils and sedimentary basins (Pinto et al. 2009, 2012; Wang et al. 2012, 2015; Hövelmann and Putnis 2016; Callagon et al. 2017; Di Lorenzo et al. 2019; Roza Llera et al. 2021). Anhydrite is highly reactive to dissolved ions. Thus, cycles of anhydrite dissolution/precipitation influence the fate of trace elements (Sr, Y, REE) in hydrothermal systems. Moreover, anhydrite surfaces effectively remove metal pollutants from aqueous solutions through coprecipitation phenomena (Morales et al. 2014; Forjanes et al. 2020b, 2020a). Pollution of running waters and aquifers by phosphorous currently is widespread due to the extensive use of ammonium phosphate as a fertilizer in intensive agriculture (Smith 2003; Wei and Bailey 2021). Understanding the processes that result from the interaction of phosphorous containing waters with common sedimentary rock-forming minerals can help to mitigate the effects of phosphorous pollution in sedimentary basins.

Moreover, apatite is a main constituent of sedimentary phosphorites (Bentor 1980; Sheldon 1981; Hughes et al. 1989; Knudsen and Gunter 2002). Baturin (1989) reported on the diagenetic origin of some apatite accumulations and connected their formation to changes in the chemistry of pore waters due to organic matter decay and sulfate reduction. The concentration of phosphorous in diagenetic fluids in pores can reach values up to 8–9 mg/L, according to Sheldon (1981). Filippelli (2002) and Dzombak and Sheldon (2020) have reported that P concentrations in young soils can reach values as high as 5340 mg/L, highlighting the potential importance of P fluxes from soils to rivers in the current scenario of climate change. In contact with the surface of sediment particles, these high concentrations are sufficient to guarantee the precipitation of apatite, which opens the question of the role that interface coupled dissolution-precipitation reactions (ICDP) may play in the formation of diagenetic apatite. It has been experimentally demonstrated that the interaction of phosphate-bearing fluids with other sedimentary rock-forming minerals like aragonite and calcite results in their replacement by aggregates of apatite crystals (Kasioptas et al. 2010, 2011; Jonas et al. 2013; Reinares-Fisac et al. 2017).

The purpose of the present work is to study the interaction of a P-bearing aqueous solution with anhydrite single crystals. The main goal is to determine the kinetics and mechanisms of anhydrite replacement by calcium phosphate at temperatures between 120 °C and 200 °C. Two calcium phosphate phases, β-TCP [β-$Ca_3(PO_4)_2$] and Hap [$Ca_5(PO_4)_3(OH)$], formed during this replacement, which were identified by Raman spectroscopy and X-ray powder diffraction (XRD). The amount of each phase as a function of temperature and reaction time was calculated by conducting the Rietveld analysis of the XRD patterns. This information was applied to determine the kinetics of the process. The textural relationships and the crystal habit of the product phases were studied by scanning electron microscopy (SEM). The influence of the transformation of β-TCP into Hap, which occurs concomitantly to the progress of the replacement, as well as the specific morphological and textural features of both calcium phosphates in the overall kinetics of the replacement reaction, was considered.

## Materials and methods

### Hydrothermal experiments

Hydrothermal interaction experiments were performed by reacting anhydrite single crystals with a 2 M $(NH_4)_2HPO_4$ aqueous solution at different reaction times (1 h to 5 days) and temperatures (120, 150, 180, and 200 °C) under pressures generated inside closed vessels (estimated pressures between 0.3 and 1.7 MPa depending on temperature). The P concentration in the aqueous solution is around 10 times higher than that reported in young soils (Filippelli 2002; Dzombak and Sheldon 2020). Anhydrite single crystals from Naica mine (Chihuahua, México) were used in all experiments. X-ray fluorescence spectroscopic analysis confirmed them as highly, with less than 0.4 wt% foreign el,ements and Sr as the major impurity. The anhydrite crystals were cleaved along {100}, {010}, and {001} using a sharp stainless-steel knife edge to obtain similarly sized (about 3 × 3 × 3 mm) anhydrite subsamples. Prior to their use in the experiments, these subsamples were cleaned in an ethanol bath to remove surface impurities and then left to dry overnight in a desiccator at room temperature. Four anhydrite subsamples (average weight ~ 250 ± 1 mg) were used in each experiment, and the volume of the solution (~4 mL) was adjusted to guarantee a solid-to-liquid ratio of 0.06 g/mL. Anhydrite subsamples were placed together with the P-bearing aqueous solution in Teflon reactors placed into steel vessels (2.5 Ø × 10 cm). Within the autoclave, all four anhydrite subsamples laid with one of their surfaces in contact with the bottom of the reactor, while their other five surfaces were directly exposed to the interaction with the P-bearing solution. The crystallographic orientation of the laying surface was not taken into consideration when setting the different experimental runs. The P-bearing aqueous solution was prepared by dissolving reagent-grade $(NH_4)_2HPO_4$ (Acros Organics) in high-purity deionized water (MilliQ) (18 MΩ cm). The pH of the fluid was measured prior to and after reaction by using a pH Meter basic 20-CRISON. Experiments were run in triplicate to confirm reproducibility. The aqueous solutions were modeled using the geochemical code PHREEQC (Parkhurst and Appelo 1999) and the llnl.dat database to calculate saturation indexes (SI) with respect to relevant solid phases at the beginning of the experiments.

After reaction, the autoclaves were removed from the oven. To accelerate their cooling to room temperature (25 °C) a flow of compressed air was applied for 20 min. The reaction time does not comprise this cooling period. Afterwards, the product samples were removed from the solution, washed with distilled water, and dried overnight at 30 °C in a thermostatic chamber. Two of the four product samples from each experiment were powdered in an agate mortar and used for powder X-ray diffraction (XRD) analyses. The other two product samples were crosscut using a steel cutter and used for Raman spectroscopy and scanning electron microscopy (SEM) imaging analyses.

### Analytical methods

Diffraction patterns of powdered product samples were measured at room temperature with a PANalytical Xpert Pro diffractometer, using a Cu$K\alpha$1 radiation. XRD data were collected in the range 7–90° 2θ with a step size of 0.001° and a dwell time of 1 s per step. Samples were hold in thin-walled glass capillaries to minimize preferential orientation effects. General peak matching runs were conducted for the diffraction patterns of product samples. These runs confirmed that in all diffraction patterns all peaks could be assigned to anhydrite (PDF 98-900-1234) and/or Hap (PDF 98-006-8592) and β-TCP (PDF 00-009-0169). Furthermore, anhydrite, Hap and β-TCP fractions in the reacted samples were determined by performing Rietveld refinement analyses using the X'Pert HighScore Plus (Ver. 3.0) software package from PANalytical. The aforementioned structural models were used as references.

Crosscut reacted samples were gold-coated and imagined using a JEOL-6610LV microscope equipped with energy-dispersive X-ray spectroscopy (EDX, INCA Energy 350). The contrast resulting from the different composition of reacted and unreacted areas provided information on the progresses of the anhydrite-(P)-bearing fluid interaction. Secondary electron images of the external surfaces of the reacted solid samples were also obtained.

Raman spectra were collected from freshly crosscut sections of the reacted subsamples. Raman spectroscopy was performed by means of a labRam HRU using JYVJobin Yvon equipment with an excitation source laser CDPS532-DPSS at 24.3 mW and excitation times of 10 s. This equipment was connected to a confocal microscope Olympus BXFM-ILHS with a 100× objective.

### Kinetic analysis

We assume that the kinetic of the replacement reaction of anhydrite by phosphate can be described by the Avrami equation (Eq. 1):

$$y_{CaP} = 1 - e^{-(kt)n} \quad (1)$$

where $y_{CaP}$ corresponds to the fraction of calcium phosphate formed ($y_{Anh} = 1 - y_{CaP}$), this is the extent of the phosphate reaction, $t$ (h) represents the reaction time, k is the Avrami rate constant (hour$^{-1}$), and $n$ is the Avrami exponent. By linearizing the Avrami equation taking twice natural logarithms, the following expression is obtained:

$$\ln[-\ln(1 - y_{CaP})] = n\ln k + n\ln t. \quad (2)$$

The Avrami equation has successfully been used to describe the kinetics of various dissolution, crystallization, transformation, and mineral replacement processes (Lasaga 1998; Xia et al. 2009; Kasioptas et al. 2010; Altree-Williams et al. 2017; Pedrosa et al. 2017). If a reaction follows the Avrami equation, different isokinetic curves will have the same n value. Moreover, their plot as $\ln[-\ln(1 - y_{CaP})]$ against $\ln t$ (Hancock-Sharp plot) will show approximately equal gradients (Hancock and Sharp 1972). Changes in the value of $n$ are indicative of changes in the mechanisms of the reaction. If the activation energy of the reaction is constant, the Hancock-Sharp plot will yield a straight line, whose slope corresponds to the value of $n$ and from whose intercept with the $y$-axis the rate constant k can be estimated. Deviations from linearity of the Hancock-Sharp plot indicate that the reaction equation differs from the Avrami one.

The rate constant k of most reactions shows a dependence of temperature that follows an Arrhenius type equation:

$$k = A \cdot e^{-E_a/R \cdot T} \quad (3)$$

where $A$ is a frequency factor, R is the gas constant, $T$ is the temperature of the experiment (Kelvin), and $E_a$ is the empirical activation energy. Taking logarithm, the Equation 4 is obtained:

$$\ln k = \ln A - E_a/RT. \quad (4)$$

If A and $E_a$ are constant, the plot of ln$k$ vs. $1/T$ is a straight line whose slope is $E_a$/R and its intercept with the $y$-axis is lnA. Thus, the value of $E_a$ can be estimated using the rate constants k derived from the Hancock-Sharp plots of a set of isothermal runs.

Commonly the empirical activation energy sums up contributions of different events involved in the reaction (dissolution of primary phases, mass transfer through interfaces, ion dehydration, nucleation, and growth of secondary phases, etc). Moreover, the method described above fails to reveal changes in the activation energy that occurs as the reaction progresses. It is possible to derive information on the evolution of the empirical activation energy $E_a$ along the reaction by rewriting Equation 3 and calculating the time required to achieve the transformation of a given fraction of the primary phase, in this case, anhydrite, into the secondary phase(s), in this case, Hap and β-TCP or a mixture of both phases, according to Equation 5:

$$t_Y \propto k^{-1} \propto A^{-1} e^{\frac{E_a}{RT}} \quad (5)$$

where $t_Y$ is the time for a given fraction to transform. This approach is described as the isoconversional method or the time to a given fraction method (Putnis 1992).

Taking logarithms, Equation 5 can be rearranged as:

$$\ln t_Y = \text{const} - \ln A + E_a/RT. \quad (6)$$

Empirical activation energies can be derived by plotting ln $t_Y$ vs. $1/T$. If there is no change in the reaction mechanism as the reaction progresses, all plots will have similar gradients and, consequently, $E_a$ will have a constant value, regardless of the given fraction transformed. On the contrary, changes in plot slopes are indicative of different mechanisms operating at different stages of the reaction, each one characterized by a different $E_a$.

## Results

### Reaction pathway and textural features

The hydrothermal interaction of anhydrite single crystals with a phosphate-bearing aqueous solution [2 M $(NH_4)_2HPO_4$] results in their partial to total transformation into Hap [$Ca_5(PO_4)_3(OH)$]. Hydroxyapatite can be accompanied by varying amounts of β-TCP [β-$Ca_3(PO_4)_2$] depending on the temperature and duration of the interaction. During the transformation, the pH of the solutions progressively decreases from an initial value of 8.1 (1) to 6.8 (1) at experiment termination time. Figure 1a depicts the XRD patterns from subsamples reacted during 6 to 72 h at 120 °C. All the diffraction patterns show sharp peaks that can be assigned to anhydrite and/or the calcium phosphate phases Hap and β-TCP. Although the XRD patterns of other calcium phosphates like whitlockite [$Ca_{18}(Mg,Fe)_2H_2PO_4]_{14}$ show similar features as the pattern of β-TCP (Gopal and Calvo 1972; Jonas et al. 2014), the formation of any amount of the former phase is disregarded, since the pristine anhydrite is highly pure and the aqueous phase contains no dissolved Fe and Mg. The intensity of anhydrite peaks progressively decreases with the reaction time. Anhydrite peaks are absent in the pattern corresponding to a reaction time of 72 h. Conversely, the intensity of peaks assigned to Hap progressively increases with time. Peaks assigned to β-TCP show a more complex evolution: their intensity initially grows to latter decrease. In all the experiments, regardless of the reaction temperature, Hap rapidly becomes the main constituent of the transformed fraction. For example, in experiments conducted at 120 °C, the transformed fraction contains ~20 wt% Hap after 12 h, 37 wt% Hap after 24 h and 73 wt% Hap after 48 h (Fig. 1b). In experiments conducted at temperatures ≥200 °C, Hap becomes the only solid phase present in the system after 10 h since the beginning of the experiment. In addition, longer experiments were carried out at temperatures below 180 °C, once the anhydrite had been completely replaced, to observe the evolution of the relative content of β-TCP and Hap in the samples. The results of these experiments indicated that the amount of β-TCP continued to decrease with time (Online Materials[1] Fig. OM1). After 5 days interaction at 120 °C, reacted samples consist of 7.2% β-TCP and 92.8 anhydrite. The Raman spectra collected on crosscut sections of reacted anhydrite subsamples indicate that all transformed rims exclusively consist of calcium phosphate phases in good agreement with the conclusions of XRD analyses. Figure 2 shows SEM images and Raman spectra taken on crosscut sections of anhydrite reacted with the P-bearing fluid at 150 °C during 12 h (Figs. 2a–2d) and 24 h (Figs. 2e–2h). The spectrum in Figure 2a shows the main vibration bands of $SO_4^{2-}$ in anhydrite: a symmetric stretching ($\nu_1$) band at 1019 cm$^{-1}$; three asymmetric stretching ($\nu_3$) bands at 1113, 1131, and 1160 cm$^{-1}$; two symmetric bending ($\nu_2$) bands at 416 and 502 cm$^{-1}$; and three asymmetric bending ($\nu_4$) bands at 610, 627, and 678 cm$^{-1}$. Raman spectra collected from transformed regions of samples reacted during 12 h (Fig. 2c) and 24 h (Figs. 2e and 2g) show bands that can be assigned to Hap: the symmetric stretching ($\nu_1$), the symmetric bending ($\nu_2$), and the asymmetric bending ($\nu_4$) vibration modes of $PO_4^{3-}$ are located at 961, 432, and 588 cm$^{-1}$, respectively. The presence of a minor broad band around 880 cm$^{-1}$ (Figs. 2c and 2e) that can be attributed to the P-OH stretching is also consistent with Hap (Penel et al. 1998). Moreover, a triplet at 1007, 1045, and 1075 cm$^{-1}$, corresponds to the $PO_4^{3-}$ asymmetric stretching ($\nu_3$) as well as a band at 3571 cm$^{-1}$ can be assigned to the OH-stretching (Fig. 2). In addition, a broad band near 946–949 cm$^{-1}$ assigned to the symmetric stretching ($\nu_1$) (Jonas et al. 2014; Pedrosa et al. 2016) indicates the presence of β-TCP in the core of the sample reacted during for 24 h (Fig. 2e). The absence of bands around 925 cm$^{-1}$ ($\nu_1$ mode) in all Raman spectra, confirms that whitlockite is not present in the system at any stage, in good agreement with the results of XRD analyses that only identify

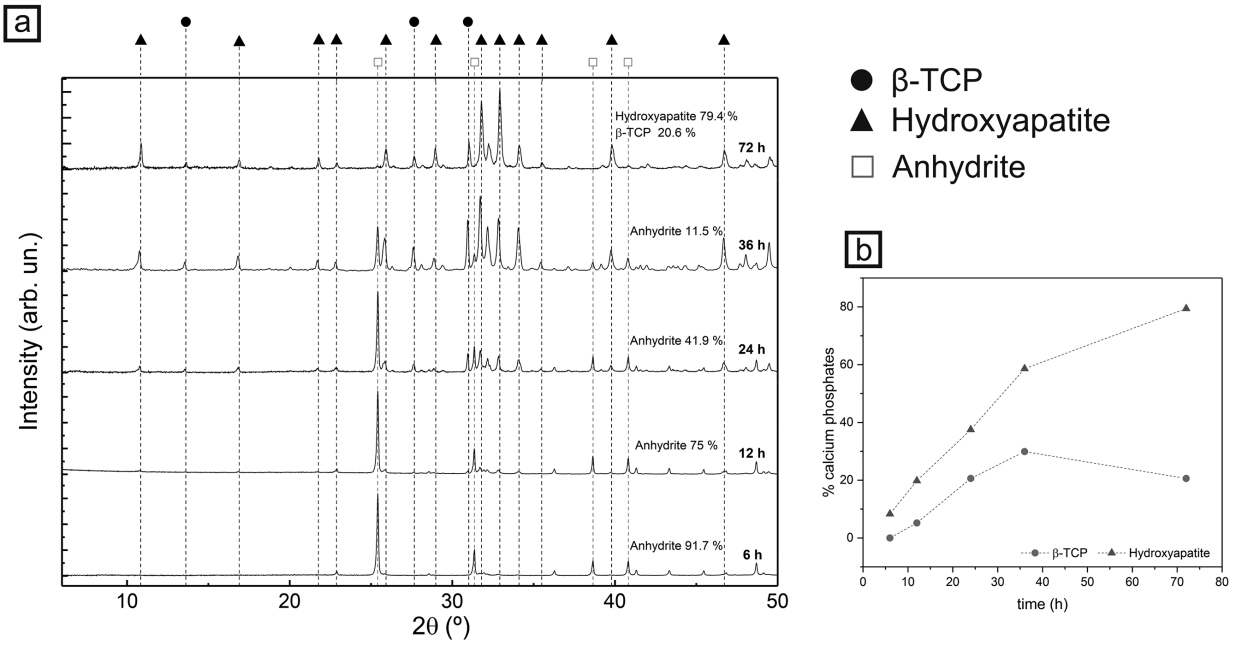


**Figure 1.** (**a**) X-ray powder diffraction patterns showing the mineralogical evolution of the replacement of anhydrite by calcium phosphates after hydrothermal interaction experiments carried out at 120 °C at different reaction times. The reflections of anhydrite, hydroxyapatite and β-TCP were marked with squares, triangles and circles, respectively. (**b**) Percent calcium phosphates, calculated by Rietveld refinement, against reaction time.

two calcium phosphate phases (β-TCP and Hap).

The main $PO_4^{3-}$ vibrational mode (ν1) in β-TCP, which is located at 971cm$^{-1}$, is not apparent in any of the Raman spectra, most likely due to overlapping with the main band in the spectra of Hap ($PO_4^{3-}$ $\nu_1$ at 961 cm$^{-1}$). No bands that can be attributed to β-TCP are present in areas close to the surface of the anhydrite sample reacted during 24 h (Fig. 2g). In summary, XRD and Raman results corroborate that the transformed samples consist of mixtures of Hap and β-TCP at early stages of the replacement reaction. At $T \geq 180$ °C, hydroxyapatite/β-tricalcium phosphate ratio rapidly increases, and hydroxyapatite is the only phase in fully replaced samples. At $T < 180$ °C hydroxyapatite/β-tricalcium phosphate ratio increases slowly. Furthermore, reacted samples still contain significant amounts of β-tricalcium phosphate even after full replacement of anhydrite is reached.

The anhydrite by calcium phosphate replacement initiates at the surface of the anhydrite subsamples and advances inwards, defining a sharp reaction front (Figs. 2b and 2d). This front defines the interface between a shell-like transformed rim and the unreacted anhydrite core (Fig. 2d). Figure 3a shows the contact between the transformed rim and the unreacted anhydrite core. As can be seen, the rim mainly consists of needle-like crystals arranged in fan-like bunches that appear oriented roughly perpendicular to the surface of the anhydrite core, and a smaller amount of euhedral rhombohedron-shaped crystals (Fig. 3a). Based on Raman spectroscopy analysis and the known crystal morphology of calcium phosphates, we interpret the needle-like crystals as Hap (Zhu et al. 2008; Kasioptas et al. 2010; Yang et al. 2014; Li et al. 2016) and the euhedral rhombohedron-shaped ones as β-TCP (Roy and Linnehan 1974). Closer inspection of the latter evidences the presence on their surfaces of dissolution pits and nanometric Hap crystals that appear to grow in close spatial relation with the dissolution pits (Fig. 3b).

Regardless the reaction temperature, the replacement reaction takes place with preservation of both the volume and external shape of the anhydrite crystals and results in the formation of calcium phosphate pseudomorphs. The pseudomorphs obtained in series of isothermal experiments were crosscut and SEM imaged. Figure 4 depicts SEM microphotographs of samples reacted during 12 h at 120 °C (a), 150 °C (b), 180 °C (c), and 200 °C (d). The transformed rim undergoes progressive thickening with increasing reaction time. The anhydrite core concomitantly shrinks. It is important to note that, before full anhydrite replacement is reached, the thickness of the transformed rim can significantly vary within each crosscut section, as is apparent in Figures 4a–4c. Differences in rim thickness, measured from opposite sides of a subsample along the same crystallographic direction, reflect the reduced exposure of the subsample surface that lies in contact with the reactor bottom to the interaction with the fluid. Differences in rim thickness measured along different crystallographic directions reflect the different reactivity of anhydrite cleavage surfaces.

As can be seen, the reaction front advances faster with increasing temperature. Thus, after 12 h of reaction, in samples reacted at 120, 150, and 180 °C, the average transformed rim thickness was 250, 550, and 1500 μm, respectively (Figs. 4a–4c). After 12 h reaction, no unreacted core is observed in the crosscut sections of samples from experiments conducted at 200 °C reacted (Fig. 4d). This is consistent with the results of both, X-ray diffraction and Raman spectroscopy analyses, which also support the complete replacement of anhydrite by calcium phosphate phases in samples reacted 12 h at 200 °C.

**Kinetics of the replacement reaction**

Several sets of hydrothermal interaction experiments were conducted to derive information on the kinetics of the replacement of anhydrite single crystals by calcium phosphate crystal aggregates. Table 1 summarizes the fraction of anhydrite, Hap and β-TCP, as determined from the Rietveld refinements of X-ray powder diffraction patterns of samples interacted with the phosphate-bearing aqueous solution at temperatures between 120 and 200 °C during times that varied between 2 and 72 h. In Figure 5, the fraction of sample transformed into calcium phosphate phases ($y_{CaP}$) is plotted against the reaction time ($t$) for each isothermal experiment. Figure 6 shows the temperature dependence of the anhydrite-by-calcium phosphate reaction, evidenced in the Hancock–Sharp plots derived by fitting the linearized Avrami expression (Eq. 2) to the experimental data. All fitted lines are approximately parallels. The Avrami parameters calculated for each set of isothermal data are also shown in Figure 6. The activation energy can be obtained by plotting the slopes of the linear regressions in Figure 6 against reciprocal temperature in an Arrhenius plot (Fig. 7). The rate constant

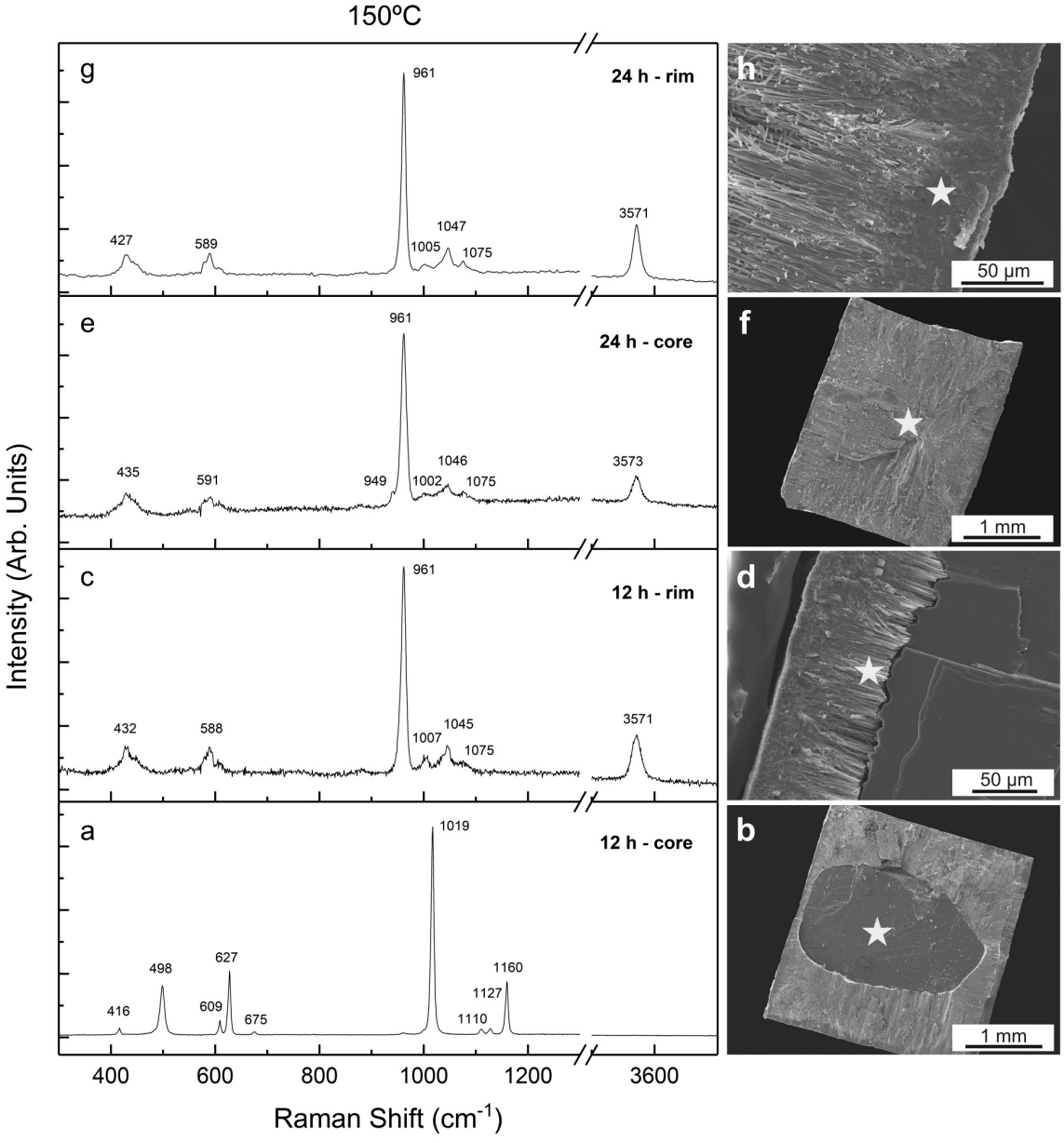


**Figure 2.** Raman spectra and SEM images of cross section of partially replaced anhydrite samples for 12 and 24 h at 150 °C. The main vibrational bands of $SO_4^{2-}$ identified (**a**) in the core of anhydrite sample reacted (**b**) match well with anhydrite. The main vibrational bands of $PO_4^{3-}$ (**c**, **e**, and **g**) identified in the rim (**d** and **h**) and core (**f**) of reacted samples corresponds to hydroxyapatite. The broad band at 949 $cm^{-1}$ and the presence of the band at 1045 $cm^{-1}$ (**d**) are characteristic of β-TCP. SEM micrographs of the reacted samples show the position where the spectra were measured.

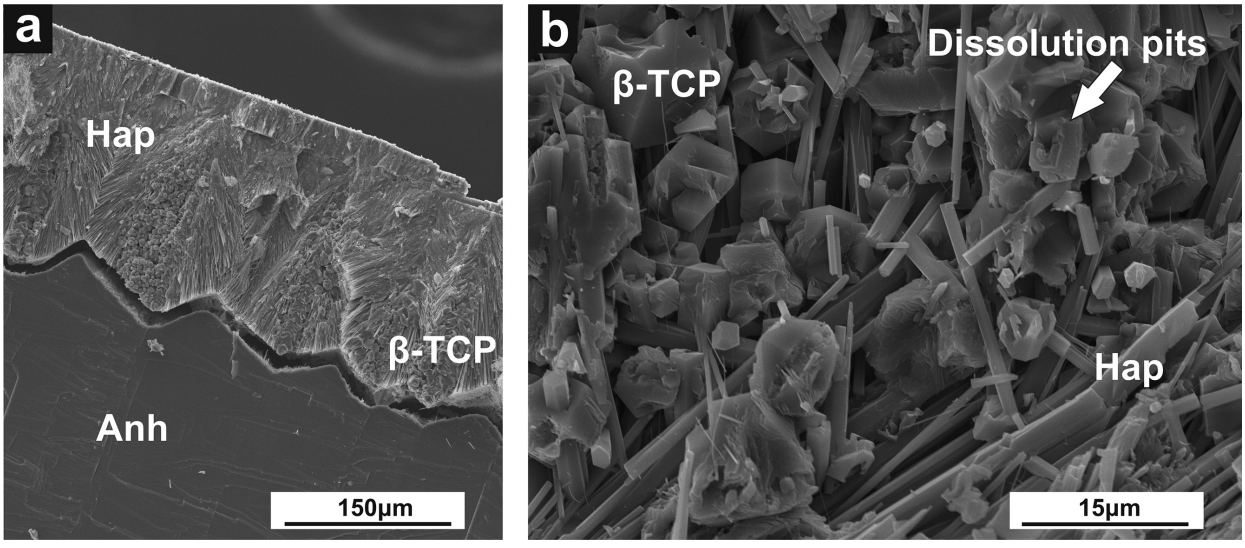


**Figure 3.** SEM micrographs of anhydrite (Anh) reacted with 2 M $(NH_4)_2HPO_4$ aqueous solution at different temperatures and reaction times. (**a**) After 3 h at 150 °C a cross cut section image shows the unreacted anhydrite core and the two calcium phosphates that can be distinguished, β-tricalcium phosphate (β-TCP) and hydroxyapatite (Hap). Hydroxyapatite is clearly more abundant and is growing in elongated hexagonal needle-like crystals that are arranged perpendicular to the unreacted anhydrite core and β-TCP shows an euhedral habit. (**b**) At higher temperatures and shorter reaction times (200 °C and 2 h), β-TCP appears with dissolution features and at the same time the development of smaller and thinner hydroxyapatite crystals from β-TCP faces.

(k) clearly increases with temperature and the linear regression yields an empirical activation energy, $E_a$ of 40.2 ± 1.9 kJ/mol.

Alternatively, empirical activation energies can also be determined by using the isoconversional method. $E_a$ values were calculated for three different fractions of anhydrite replacement by calcium phosphate, 0.40, 0.60, and 0.80 (Fig. 8). In all cases, the data are well described by linear correlations and show closely parallel trends. The empirical $E_a$ values yielded from these fittings slightly decreases, from 40.4 ± 2.3 to 39.3 ± 2.3 kJ·mol$^{-1}$, as the replaced fraction increases from 40 to 80%.

## Discussion

### Replacement reaction mechanism

Upon interaction with a P-bearing aqueous solution at temperatures between 120 and 200 °C, anhydrite single crystals are replaced by mixtures of β-TCP and Hap. Textural features of the reacted samples are consistent with the replacement taking place through an interface coupled dissolution-reprecipitation reaction (Putnis 2002, 2009; Putnis and Putnis 2007; Ruiz-Agudo et al. 2014). First, the reaction starts at the surface of anhydrite and progresses from rim to core through the advancement of a reaction front that appears sharp, well-defined, and approximately parallel to the original anhydrite surface. Second, the external shape as well as most surface features of anhydrite crystals are preserved throughout the reaction, which has a pseudomorphic character. Third, replaced samples consist of aggregates of crystals of the product phases and contain large amounts of porosity. All these features are characteristic of mineral replacement processes that occur mediated by the presence of a fluid phase. The reaction takes place in the interfacial layer of fluid. When the process starts, the fluid is undersaturated with respect to the primary phase. This drives its dissolution and determines that the interfacial layer of fluid soon becomes supersaturated with respect to the product(s). Anhydrite dissolution releases $Ca^{2+}$ and $SO_4^{2-}$ ions to the interfacial layer of fluid. To evaluate the physicochemical conditions in the interfacial fluid at early stages of replacement process, we simulate the dissolution of a small amount of anhydrite in a small volume of fluid using the geochemical code PHREEQC and the lnll.dat database (Parkhurst and Appelo 1999). We consider the successive dissolution of layers of anhydrite whose thickness corresponds to one unit cell ($a_0$ = 6.993 Å, $b_0$ = 6.995 Å, and $c_0$ = 6.245 Å; Hawthorne and Ferguson 1975). For a 3 × 3 × 3 mm sized crystal, the dissolved anhydrite volume is 3.64 × 10$^{-8}$ cm$^3$ of $CaSO_4$, which corresponds to 7.94 × 10$^{-10}$ moles of anhydrite. We consider two realistic thicknesses for the fluid boundary layer, 100 and 1000 nm, which corresponds to a volume of interfacial solution of 5.4 × 10$^{-6}$ cm$^3$ and 5.4 × 10$^{-5}$ cm$^3$, respectively (Ruiz-Agudo et al. 2015). The state of supersaturation is defined by the value of the saturation index (SI), which is expressed as:

$$SI = \log (IAP/Ksp) \quad (7)$$

where IAP is the ion activity product, and Ksp is the solubility product of the phase considered. SI = 0 indicates that the system is in equilibrium with a given phase; this is saturated, while SI < 0 and SI > = 0 indicate that the system is undersaturated and supersaturated, respectively. At 150 °C, the dissolution of one anhydrite monolayer in both 100 and 1000 nm boundary layers results in the interfacial fluid layer becoming supersaturated with respect to Hap and β-TCP. Thus, the 100 nm thick boundary layer becomes supersaturated with respect to both, Hap and β-TCP ($SI_{Hap}$ = 23.86, $SI_{β\text{-}TCP}$ = 3.42) after the dissolution of one anhydrite monolayer while still remaining undersaturated with respect to

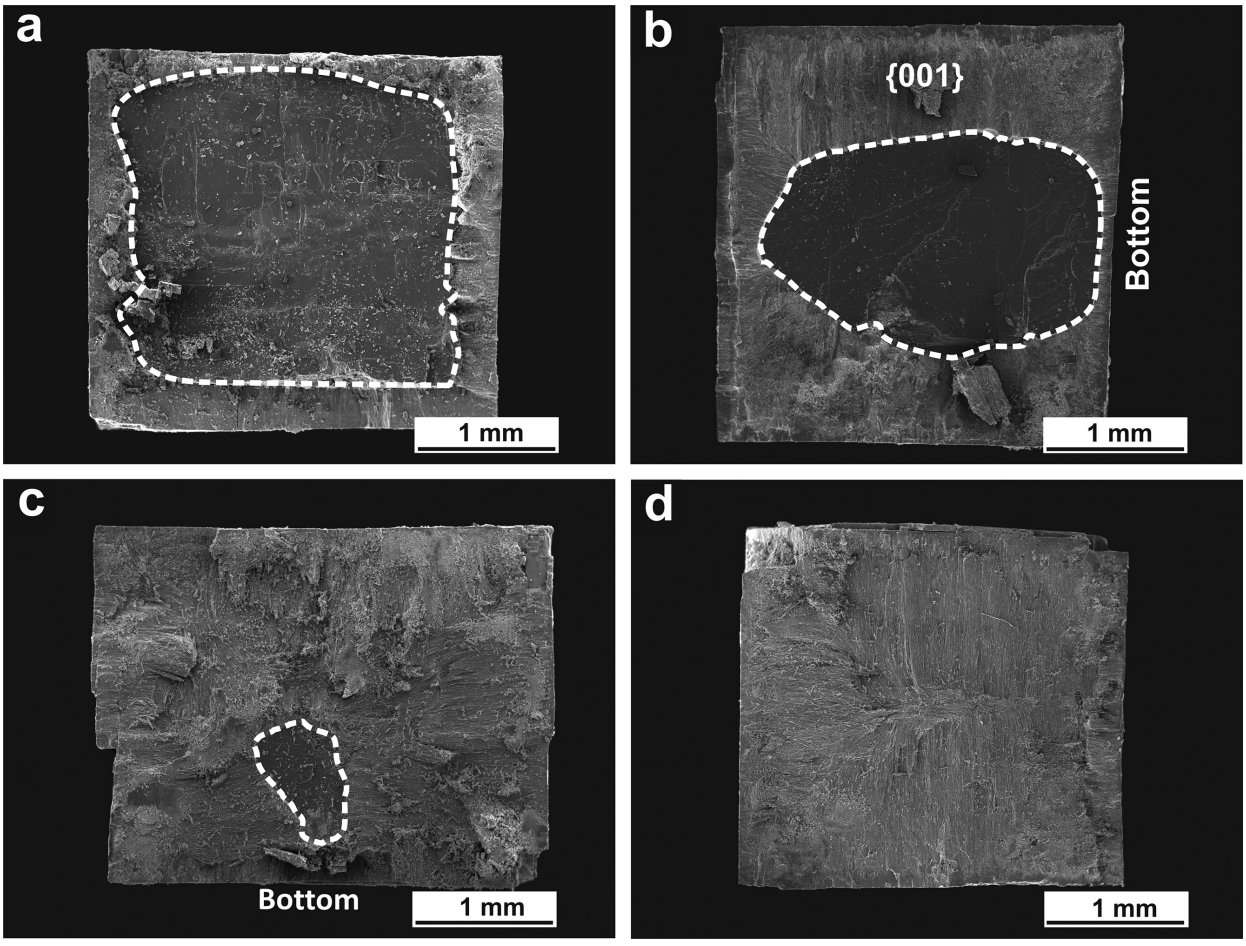


**Figure 4.** SEM micrographs of cross sections surfaces showing the anhydrite replacement by calcium phosphates after 12 h of reaction at temperatures of 120 (**a**), 150 (**b**), 180 (**c**), and 200 (**d**).

this latter phase ($SI_{Anh}$ = –7.36). Similarly, the 1000 nm thick boundary layer reaches supersaturation with respect to Hap and β-TCP ($SI_{Hap}$ = 19.11, $SI_{β\text{-}TCP}$ = 0.56) after the dissolution of one anhydrite monolayer. The simulation of the dissolution of one anhydrite monolayer at other experimental temperatures also yields SI > 0 for both, Hap and β-TCP. The SI value for all the phases involved increases as successive anhydrite monolayers dissolve. Once the interfacial fluid reaches the supersaturation threshold for Hap and β-TCP nucleation, both calcium phosphate phases will precipitate at the reaction front. As a replaced rim forms, the presence of pores within it guarantees a continuous communication between the bulk solution and the reaction front, facilitating mass transport to and from the interface (Putnis et al. 2005; Putnis and Putnis 2007; Pollok et al. 2011; Forjanes et al. 2020b). The progress of the reaction involves the definition of a dissolution-crystallization feedback loop. Thus, anhydrite dissolution promotes calcium phosphate precipitation in the interfacial fluid and vice versa. The preservation of the external shape of anhydrite crystals requires that the rates of anhydrite dissolution and calcium phosphate precipitation are coupled (Putnis 2002, 2009; Putnis and Putnis 2007; Pollok et al. 2011; Ruiz-Agudo et al. 2014). In the temperature range of the experiments, the solubility product of anhydrite varies between $10^{-4.36}$ at 120 °C and $10^{-4.83}$ at 200 °C (Freyer and Voigt 2003). The solubility product

**Table 1.** Calculated transformation (% calcium phosphates) calculated by Rietveld refinement of X-ray diffraction patterns during hydrothermal experiment

| 120 °C | | | | 150 °C | | | | 180 °C | | | | 200 °C | | | |
|---|---|---|---|---|---|---|---|---|---|---|---|---|---|---|---|
| *t* (h) | % Anh | % β-TCP | % Hap | *t* (h) | % Anh | % β-TCP | % Hap | *t* (h) | % Anh | % β-TCP | % Hap | *t* (h) | % Anh | % β-TCP | % Hap |
| 6 | 91.7 | | 8.3 | 3 | 78.5 | 3.2 | 18.3 | 2 | 73.5 | 12.9 | 13.6 | 2 | 58.8 | 27.1 | 14.1 |
| 12 | 75 | 5.2 | 19.8 | 6 | 48.4 | 20.4 | 31.3 | 4 | 40.3 | 21.9 | 37.9 | 4 | 26.8 | 6.6 | 66.7 |
| 24 | 41.9 | 20.6 | 37.5 | 8 | 41 | 22.5 | 36.5 | 6 | 20 | 16.7 | 63.3 | 6 | 8.9 | 4.4 | 86.7 |
| 36 | 11.5 | 29.9 | 58.6 | 12 | 19.8 | 21.1 | 59.2 | 8 | 8.2 | 7.7 | 84.2 | 10 | 0 | 0 | 100 |
| 48 | 9.5 | 17.2 | 73.3 | 20 | 0 | 13.5 | 86.5 | 10 | 6.1 | 3.9 | 90 | | | | |
| 72 | | 20.6 | 79.4 | | | | | 12 | 4.1 | 2 | 93.9 | | | | |
| | | | | | | | | 14 | 0 | 0 | 100 | | | | |

[a] $R_{wp}$ is ~10% in all refinements.

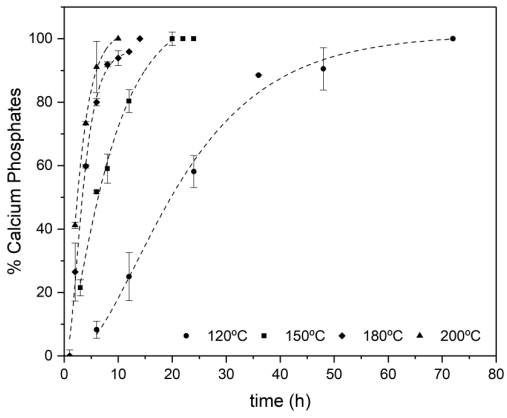


**Figure 5.** Fraction of calcium phosphates replacing anhydrite crystals against the reaction time for each isothermal experiments. The lines are fitted to the Chapman equation.

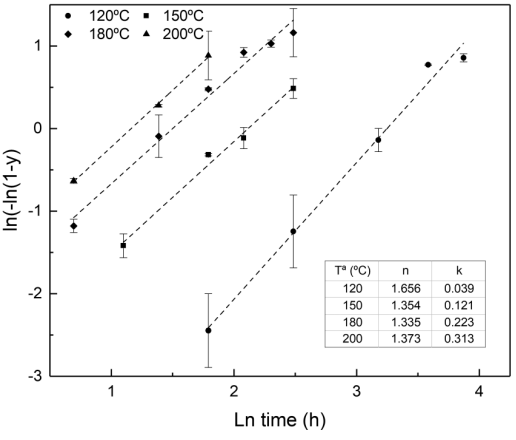


**Figure 6.** Plot of the calcium phosphates transformed fraction (y) vs. time. From the slope and the intercept, Avrami rate low parameters (n and k) are determined.

of Hap strongly decreases with increasing temperature within this temperature range, being $10^{-58.33}$ at 120 °C and $10^{-70.64}$ at 200 °C (Kaufman and Kleinberg 1979). In contrast, the solubility product of β-TCP slightly increases with temperature in the temperature range of the experiments from $10^{-26.63}$ at 120 °C to $10^{-25.42}$ at 200 °C (Wang and Nancollas 2008). Considering the very large differences in solubility between anhydrite and both calcium phosphates, it is likely that the latter phases form under very high supersaturations, and it can be expected that this process occurs rapidly at any experimental temperature. Therefore, anhydrite dissolution is most likely the rate-limiting process. However, the progress of the reaction requires continuous chemical exchange with the bulk solution, and the rate of mass transport through the porous replaced rim may play a significant role in modulating the overall kinetics of the anhydrite by calcium phosphate replacement reaction.

## Reaction pathway

The mole ratio of β-TCP/Hap vary with temperature and reaction time. At 120 °C, β-TCP/Hap mole ratio first increases

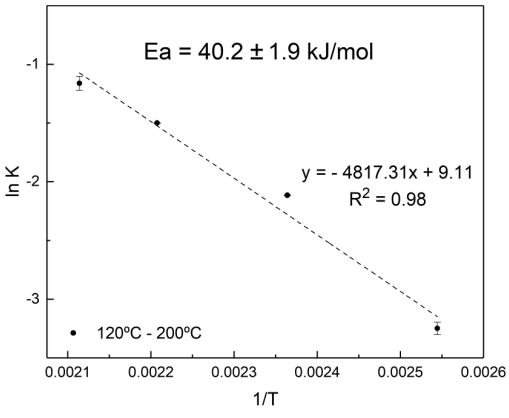


**Figure 7.** Linear fitting of the rate constant K vs. the reciprocal of temperature (expressed in Kelvin).

with reaction time and later slowly decreases. At all other temperatures β-TCP/Hap mole ratio progressively decreases with increasing reaction time. This decrease takes place much more rapidly with increasing temperature. In the temperature range of the experiments, β-TCP is more soluble than Hap (llnl.dat) and, consequently, less stable. Therefore, β-TCP forms as a thermodynamically metastable phase. Crystallization of metastable phases often occurs under high supersaturations. The large solubility difference between anhydrite, β-TCP and Hap determines that the layer of fluid at the interface will be very highly supersaturated with respect to both, β-TCP and Hap. Under these conditions, both calcium phosphate phases can nucleate. Indeed, the presence of Hap at very early stages of the replacement process suggests a competition between the nucleation and growth of β-TCP and Hap. Metastable β-TCP latter transforms into Hap according to an Ostwald ripening process. This transformation most likely occurs through a dissolution-reprecipitation reaction since dissolution pits are apparent in the surface of β-TCP and needle-like Hap crystals grow spatially associated to those pits (Fig. 3b). The competition between the nucleation and growth of β-TCP and Hap operates longer and plays a more important role at lower temperatures as is evidenced by the initial increase in the β-TCP/Hap mole ratio as well as the large amount of β-TCP in almost fully replaced samples at 120 °C.

The replacement reaction can be described through the following equations:

$$3CaSO_4 + 2(NH_4)_2HPO_4(aq) \rightarrow Ca_3(PO_4)_2 + (NH_4)_2SO_4(aq) + 2(NH_4)HSO_4(aq) \quad (8)$$

$$5CaSO_4 + 3(NH_4)_2HPO_4(aq) + H_2O \rightarrow Ca_5(PO_4)_3OH + (NH_4)_2SO_4(aq) + 4(NH_4)HSO_4(aq) \quad (9)$$

$$5Ca_3(PO_4)_2 + 3H_2O \rightarrow 3Ca_5(PO_4)_3OH + H_3PO_4(aq) \quad (10)$$

The precipitation of Hap, as a basic salt, results in a pH decrease in the fluid phase (Eqs. 9 and 10). This is in good agreement with the change from an initial $pH_i = 8.1$ (1) to a pH of 6.8 (1) measured at the end of the experiments.

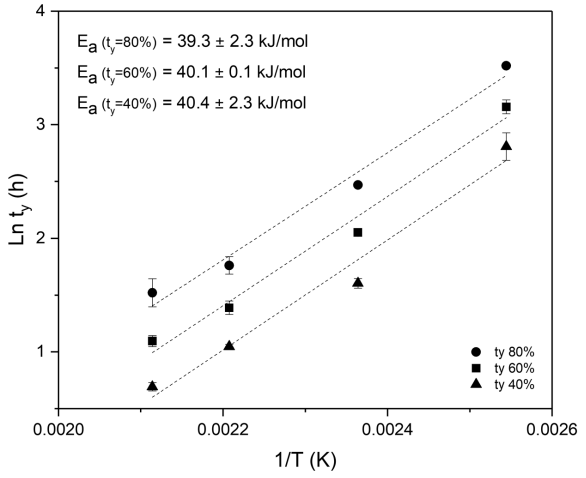


**Figure 8.** Experimental data of the time ($\ln t_y$) for several fractions (Y = 40, 60, and 80%) of transformed anhydrite vs. 1/*T*. The slope of the fitting straight lines corresponds to $E_a$/R.

### Porosity generation

Several factors explain the generation of porosity during pseudomorphic replacement reactions. Porosity balances the loss of volume in reactions that involve a negative molar volume change and guarantees the preservation of the original external shape of the primary phase. In the case of the replacement of anhydrite ($V_{Anh}$ = 45.84 cm$^3$/mol) by mixtures of β-TCP ($V_{β\text{-}TCP}$ = 33.14) and Hap ($V_{Hap}$ = 31.79 cm$^3$/mol), all relevant molar volume changes are negative: –12.70 cm$^3$/mol (27.7%) and –14.05 (30.65%), the changes associated to the transformation of anhydrite into β-TCP and Hap, respectively, and –1.35 (4.07%) the change associated to the transformation of β-TCP into Hap. These molar volume changes only very slightly vary (<1%) depending on the experimental temperature (Evans 1979; Nakamura et al. 1990). The porosity required to balance the molar volume change associated to the replacement reaction will be around 30%, although the exact value will vary depending on the β-TCP/Hap mole ratio in the calcium phosphate mixture. Since this ratio changes with reaction time and temperature, small differences in porosity can be expected depending on the experimental conditions.

A second source of porosity is the difference in solubility between the primary and product phases (Putnis 2002, 2009; Pollok et al. 2011). β-TCP and Hap are less soluble than anhydrite. This means that part of the dissolved anhydrite is lost to the solution when this phase is replaced by β-TCP and Hap. The negative solubility change associated with the replacement will also be balanced by the generation of porosity that will add up to that that balances the negative molar volume change. The volume of solubility change-related porosity is also influenced by reaction time and temperature, as both parameters determine the β-TCP/Hap in the reacted sample. Differences in the porosity formed during the replacement may influence the mass transport rate and be reflected by the overall kinetics of the replacement reaction (Jonas et al. 2013; Pedrosa et al. 2017).

### Textural features and evolution

Mass transport from and to the interface is not only affected by the increase of porosity during the replacement but also by the specific characteristics of this porosity regarding pore shape, size and connectivity (Putnis et al. 2005; Jonas et al. 2013; Putnis 2015; Yuan et al. 2018; Forjanes et al. 2020a). Yuan et al. (2018) studied the porosity generated during the replacement of calcite by cerussite and identified three types of pores: Open pores that directly connect the reaction front and the bulk solution, trapped pores, which are connected through grain boundary diffusion between the crystals of the product phase and open pores to the bulk solution, and isolated pores, located between differently oriented crystals of the product. All types of pores are filled by fluid, but the chemistry of this fluid will vary due to differences in the mass transport rate. Chemical exchange between the interfacial fluid and the bulk will be more efficient if the porosity mainly consists of open pores, while the predominance of isolated pores will strongly hinder mass transport and the progress of the reaction. Both habit and textural relationships of the product crystals are key features that define the relative amount of open, trapped and isolated pores in replaced samples. The existence/absence of epitactic relationships between the product and the primary phase is another key factor. We observe no evidence of epitatic growth of either β-TCP or Hap on anhydrite surfaces. β-TCP crystals grow randomly oriented, while Hap grow as fan-like bunches of needle-like crystals arranged approximately perpendicular to the anhydrite surface (Fig. 3). β-TCP crystals accumulated in the central region of this bunches. Needle-like crystals within bunches that seem to originate at the region occupied by β-TCP crystals are arranged with their long axis approximately parallel between them. This arrangement is characteristic of competitive growth between crystals that nucleate randomly oriented on a surface and have a preferential growth direction. Those crystals oriented with the preferential growth direction perpendicular to the surface can grow freely, while the growth of all differently oriented crystals rapidly becomes prevented by the lack of space. It is noteworthy that the porosity generated during replacement reactions has a transient nature, and its features evolve along time. In the case of the replacement of anhydrite by calcium phosphate, the very different habit of β-TCP and Hap crystals will determine differences in the relative abundance of different types of pores depending on the mole β-TCP/Hap ratio in the replaced sample. As pores between elongated, parallel crystals tend to be open, it can be expected that the number of open pores in replaced samples will increase as more β-TCP transforms into Hap.

### Rate-limiting process

Coupled dissolution-precipitation reactions are heterogeneous processes. Their kinetics is either limited by the dissolution of the primary phase or by the precipitation of the product phase(s). Several observations give support to the interpretation that the dissolution of anhydrite is the limiting step of the anhydrite by calcium phosphate replacement reaction. Moreover, textural features of the reacted samples indicate that the reaction progresses from rim to core. This has been interpreted by different authors as evidence of the precipitation of the product(s) taking place at a faster rate than the dissolution of the primary phase. Altree-Williams et al. (2015, 2017) pointed out that mineral replacement reactions that are rate-limited by the precipitation of the product also result in the formation of pseudomorphs. However, external features of these pseudomorphs are less ac-

curately preserved as the formation of overgrowths blurs them. Moreover, these pseudomorphs show hollow cores. Neither the development of overgrowths nor the formation of a hollow core is observed during the formation of calcium phosphate pseudomorphs after anhydrite.

Altree-Williams et al. (2019) calculated an average empirical activation energy ($E_a$) of 46.2 ± 7.6 kJ/mol for the carbonation of anhydrite. These authors interpreted the slightly lower value of this activation energy compared to previously reported values of the activation energy for anhydrite dissolution [50 kJ/mol, Bildstein et al. (2001); 61.0 ± 1.0 kJ/mol, Kontrec et al. (2002)] as indicative of anhydrite dissolution being the rate-limiting event of anhydrite carbonation kinetics. Moreover, they concluded that, since the reported values of the activation energy for the diffusion of dissolved calcium are much smaller ($E_a$ = 12.6 kJ/mol), mass transport of species from the bulk solution to the reaction interface and backward must occur a faster rate compared to anhydrite dissolution. The average empirical activation energy of the anhydrite by calcium phosphate replacement reaction determined in this work using the isoconversional method is 39.9 ± 1.6 kJ/mol. The similarity of this value to the previously reported activation energy for anhydrite carbonation supports that anhydrite dissolution also controls the kinetics of anhydrite phosphation.

The experimental data fitted with the Avrami model yields an $E_a$ = 40.2 ± 1.9 kJ/mol, which is identical to that obtained using the isoconversional method regardless of the transformed fraction considered. The calculated A is 9045.3 $(h)^{-1}$, and the resulting integral law is $y_{CaP} = 9045.3e^{(-40/RT)}t$. Applying the law equation and assuming that the reaction mechanism is the same as that controlling the process in the 120–200 °C range, it can be estimated that at 20 °C the time required to for the complete replacement of anhydrite single crystals by calcium phosphate will be around 4 months. However, similar experiments performed under lower temperature conditions need to be performed to confirm the soundness of this approach.

The shape of the rate curves in Figure 5 is approximately the same for those corresponding to 150, 180, and 200 °C, and the curves can be described as isokinetic. Consistently, the Avrami reaction exponents ($n$) corresponding to these three temperatures show almost identical values (~1.35). The shape of the rate curve corresponding to 120 °C is slightly different, which correlates with a larger Avrami exponent (~1.66 at 120 °C) (Fig. 5). The value of Avrami exponents is characteristic of the rate-limiting kinetic mechanism that operates at each temperature (Redfern 1987). All calculated Avrami exponents in this work stand between those defined by Hancock and Sharp (1972) for first-order and higher-order processes. However, it is important to keep in mind that Hancock and Sharp (1972) studied solid-state transformations, while the replacement of anhydrite by calcium phosphate phase takes place mediated by the presence of a fluid phase. Several authors have interpreted changes in the value of the Avrami exponent with temperature as reflecting a balance between changes in the solubilities of the primary and secondary phases combined with changes that affect mass transport processes (Zhao et al. 2009; Altree-Williams et al. 2019). The solubility of anhydrite and apatite decreases with increasing temperature. However, this decrease follows a different trend depending on the phase (Gregory et al. 1974; McDowell et al. 1977; Otálora and García-Ruiz 2014; llnl database from PHREEQC code). Moreover, in the temperature range of the experiments the solubility of β-TCP shows a positive dependence with temperature. These differences in solubility evolution may be reflected by the Avrami exponent. The replacement of ahnydrite by calcium phosphates does not only involve the dissolution of anhydrite to form Hap. β-TCP precipitation is metastable and, as the reaction progresses, β-TCP dissolves to form Hap. The formation of β-TCP and its transformation into Hap may also weigh differently on the overall kinetics of the replacement depending on the reaction temperature. Reported values of the empirical activation energy of β-TCP dissolution are around 16.3 kJ/mol, which is much smaller a value than that of the activation energy for the dissolution of anhydrite and very close to the activation energy for the diffusion of dissolved calcium (Bohner et al. 1997). Although its activation energy is small, the influence of β-TCP dissolution may sufficiently influence the kinetics of Hap formation as to explain changes in the Avrami exponent. Moreover, the β-TCP into Hap transformation differently affect textural features of the reacted samples depending on the temperature. After complete replacement of anhydrite by calcium phosphate, β-TCP content is highest in samples reacted at 120 °C (~20%), followed by those reacted at 150 °C (~13%). Given the very different morphology of β-TCP crystals compared to those of hydroxyapatite as well as the slightly larger molar volume of the former, differences in porosity and pores arrangement may further explain small kinetics changes at different reaction temperatures (Putnis et al. 2005; Jonas et al. 2013; Putnis 2015; Pedrosa et al. 2017).

## Implications

In this work, we have analyzed the kinetics of the replacement of anhydrite single crystals by mixtures of the calcium phosphates phases, β-TCP and Hap, via a dissolution-precipitation reaction that takes place under hydrothermal conditions (from 120 to 200 °C). The fitting of the experimental results to both the Avrami equation and the isoconversional method yields experimental activation energies, $E_a$, around 40 kJ/mol. This value is similar to that determined by Altree-Williams et al. (2019) for the carbonation of anhydrite, which is rate-limited by anhydrite dissolution. However, Avrami exponents stand between those defined by Hancock and Sharp (1972) for first-order and higher-order processes. We interpret that this apparent contradiction reflects the complexity of coupled dissolution-precipitation reactions, whose kinetics are modulated by several factors, including the dissolution rate of the primary phase, the volume, connectivity, and permeability of the porosity formed during the replacement, the precipitation rate of the secondary phase(s) and the textural evolution of the latter. In the case under consideration, we conclude that there exists a competition between the nucleation and growth of β-TCP and Hap at the early stages of the replacement, which last longer the lower the reaction temperature is. Due to the very different morphological features of β-TCP and Hap crystals, this competition strongly influences the texture of the replacement, its pores arrangement, and, thereby, the mass transfer from and to the interfacial fluid, which emphasizes the important role of metastable precursor phases and Ostwald ripening processes in

defining the overall kinetics of coupled dissolution-precipitation reactions. The results of this study indicated that the replacement of sedimentary rock-forming minerals during diagenesis is a feasible mechanism for the formation of some calcium phosphate accumulations in sedimentary basins. In this study, anhydrite single crystals were used. Anhydrite sedimentary rocks are polycrystalline materials that consist of grains bounded by differently oriented crystal surfaces. The reactivity of these surfaces may differ from that of the anhydrite cleavage surfaces. Moreover, the presence of differently oriented crystal surfaces may facilitate the epitactic growth of the product phases on the parent phase substrate. It is well established that the formation of epitactic overgrowths contributes to passivate the substrate and commonly hinders the progress of replacement reactions (Rodríguez-Blanco et al. 2007; Forjanes et al. 2020a). On the other hand, the network of grain boundaries in rocks facilitates fluid infiltration and provides an increased reactive surface compared to a single crystal, which may influence the reaction mechanism (Jonas et al. 2013, 2014). Future experimental work using anhydrite evaporitic rock samples will help to elucidate this influence. The results of this study also shed light on the mechanisms involved in the removal and immobilization of an important pollutant, P, by mineral surfaces. Due to the main role of P in the life cycle, the scarcity of this element in the Earth's crust, and its ability to pollute soils, sediments, and ground and running waters, developing methods for the recovery of P through the precipitation of phosphate phases on the surface of pre-existing minerals would have outstanding importance. The results of this study, together with further experimental work using polycrystalline samples and fluids with P concentrations closer to those found in natural environments, can contribute to reaching this goal.

## Acknowledgments and Funding

The authors thank Emilio Matesanz (CAI Rayos X, Complutense University of Madrid) and the SCTs (University of Oviedo) for providing excellent technical support and assistance. This study was supported by the Ministry of Science, Innovation and Universities (CIENCIA) (Spain) under projects CGL2016-77138-C2-1-P, CGL2016-77138-C2-2-P, and PID2021-125467NB-I00. A.R. acknowledges funding through contract BES-2017-081759 from the Spanish Science Ministry.

## References cited

Altree-Williams, A., Pring, A., Ngothai, Y., and Brugger, J. (2015) Textural and compositional complexities resulting from coupled dissolution-reprecipitation reactions in geomaterials. Earth-Science Reviews, 150, 628–651, https://doi.org/10.1016/j.earscirev.2015.08.013.

——— (2017) The carbonatation of anhydrite: Kinetics and reaction pathways. ACS Earth & Space Chemistry, 1, 89–100, https://doi.org/10.1021/acsearthspacechem.6b00012.

Altree-Williams, A., Brugger, J., Pring, A., and Bedrikovetsky, P. (2019) Coupled reactive flow and dissolution with changing reactive surface and porosity. Chemical Engineering Science, 206, 289–304, https://doi.org/10.1016/j.ces.2019.05.016.

Baturin, G. (1989) The origin of marine phosphorites. International Geology Review, 31, 327–342, https://doi.org/10.1080/00206818909465885.

Bentor, Y. (1980) Phosphorites—The unsolved problems. In Y. Bentor, Ed., Marine Phosphorites-Geochemistry, Occurrence. Genesis, 29, 3–18. SEPM Society for Sedimentary Geology.

Bildstein, O., Worden, R., and Brosse, E. (2001) Assessment of anhydrite dissolution as the rate-limiting step during thermochemical sulfate reduction. Chemical Geology, 176, 173–189, https://doi.org/10.1016/S0009-2541(00)00398-3.

Bohner, M., Lemaître, J., and Ring, T.A. (1997) Kinetics of dissolution of β-tricalcium phosphate. Journal of Colloid and Interface Science, 190, 37–48, https://doi.org/10.1006/jcis.1997.4846.

Callagon, E.B.R., Lee, S.S., Eng, P.J., Laanait, N., Sturchio, N.C., Nagy, K.L., and Fenter, P. (2017) Heteroepitaxial growth of cadmium carbonate at dolomite and calcite surfaces: Mechanisms and rates. Geochimica et Cosmochimica Acta, 205, 360–380, https://doi.org/10.1016/j.gca.2016.12.007.

Di Lorenzo, F., Ruiz-Agudo, C., and Churakov, S.V. (2019) The key effects of polymorphism during Pb II uptake by calcite and aragonite. CrystEngComm, 21, 6145–6155, https://doi.org/10.1039/C9CE01040H.

Dzombak, R.M. and Sheldon, N.D. (2020) Weathering Intensity and presence of vegetation are key controls on soil phosphorus concentrations: Implications for past and future terrestrial ecosystems. Soil Systems, 4, 73, https://doi.org/10.3390/soilsystems4040073.

Evans, H.T. Jr. (1979) The thermal expansion of anhydrite to 1000 °C. Physics and Chemistry of Minerals, 4, 77–82, https://doi.org/10.1007/BF00308361.

Ewing, R.C. and Wang, L. (2002) Phosphates as nuclear waste forms. Reviews in Mineralogy and Geochemistry, 48, 673–699, https://doi.org/10.2138/rmg.2002.48.18.

Filippelli, G.M. (2002) The global phosphorus cycle. Reviews in Mineralogy and Geochemistry, 48, 391–425, https://doi.org/10.2138/rmg.2002.48.10.

Forjanes, P., Gómez-Barreiro, J., Morales, J., Astilleros, J.M., and Fernández-Díaz, L. (2020a) Epitactic growth of celestite on anhydrite: Substrate induced twinning and morphological evolution of aggregates. CrystEngComm, 22, 5743–5759, https://doi.org/10.1039/D0CE00755B.

Forjanes, P., Astilleros, J.M., and Fernández-Díaz, L. (2020b) The formation of barite and celestite through the replacement of gypsum. Minerals, 10, 189, https://doi.org/10.3390/min10020189.

Freyer, D., and Voigt, W. (2003) Crystallization and phase stability of $CaSO_4$ and $CaSO_4$—Based Salts. Monatshefte für Chemie/Chemical Monthly, 134, 693–719.

Gopal, R. and Calvo, C. (1972) Structural relationship of whitlockite and $\beta Ca_3(PO_4)_2$. Nature. Physical Science, 237, 30–32, https://doi.org/10.1038/physci237030a0.

Gregory, T., Moreno, E., Patel, J., and Brown, W. (1974) Solubility of $\beta$-$Ca_3(PO_4)_2$ in the system $Ca(OH)_2$-$H_3PO_4$-$H_2O$ at 5, 15, 25, and 37 °C. Journal of Research of the National Bureau of Standards: Physics and Chemistry, 78, 667–674, https://doi.org/10.6028/jres.078A.042.

Hancock, J.D. and Sharp, J.H. (1972) Method of comparing solid-state kinetic data and its application to the decomposition of kaolinite, brucite, and $BaCO_3$. Journal of the American Ceramic Society, 55, 74–77, https://doi.org/10.1111/j.1151-2916.1972.tb11213.x.

Hawthorne, F. and Ferguson, R. (1975) Anhydrous sulphates; II, Refinement of the crystal structure of anhydrite. Canadian Mineralogist, 13, 289–292.

Hövelmann, J. and Putnis, C.V. (2016) In situ nanoscale imaging of struvite formation during the dissolution of natural brucite: Implications for phosphorus recovery from wastewaters. Environmental Science & Technology, 50, 13032–13041, https://doi.org/10.1021/acs.est.6b04623.

Hughes, J.M., Cameron, M., and Crowley, K.D. (1989) Structural variations in natural F, OH, and Cl apatites. American Mineralogist, 74, 870–876.

Jonas, L., John, T., and Putnis, A. (2013) Influence of temperature and Cl on the hydrothermal replacement of calcite by apatite and the development of porous microstructures. American Mineralogist, 98, 1516–1525, https://doi.org/10.2138/am.2013.4288.

Jonas, L., John, T., King, H.E., Geisler, T., and Putnis, A. (2014) The role of grain boundaries and transient porosity in rocks as fluid pathways for reaction front propagation. Earth and Planetary Science Letters, 386, 64–74, https://doi.org/10.1016/j.epsl.2013.10.050.

Kasioptas, A., Geisler, T., Putnis, C.V., Perdikouri, C., and Putnis, A. (2010) Crystal growth of apatite by replacement of an aragonite precursor. Journal of Crystal Growth, 312, 2431–2440, https://doi.org/10.1016/j.jcrysgro.2010.05.014.

Kasioptas, A., Geisler, T., Perdikouri, C., Trepmann, C., Gussone, N., and Putnis, A. (2011) Polycrystalline apatite synthesized by hydrothermal replacement of calcium carbonates. Geochimica et Cosmochimica Acta, 75, 3486–3500, https://doi.org/10.1016/j.gca.2011.03.027.

Kaufman, H.W. and Kleinberg, I. (1979) Studies on the incongruent solubility of hydroxyapatite. Calcified Tissue International, 27, 143–151, https://doi.org/10.1007/BF02441177.

Knudsen, A.C. and Gunter, M.E. (2002) Sedimentary phosphorites—An example: Phosphoria formation, Southeastern Idaho, U.S.A. Reviews in Mineralogy and Geochemistry, 48, 363–389, https://doi.org/10.2138/rmg.2002.48.9.

Kontrec, J., Kralj, D., and Brečević, L. (2002) Transformation of anhydrous calcium sulphate into calcium sulphate dihydrate in aqueous solutions. Journal of Crystal Growth, 240, 203–211, https://doi.org/10.1016/S0022-0248(02)00858-8.

Kuhn, T., Herzig, P.M., Hannington, M.D., Garbe-Schönberg, D., and Stoffers, P. (2003) Origin of fluids and anhydrite precipitation in the sediment-hosted Grimsey hydrothermal field north of Iceland. Chemical Geology, 202, 5–21, https://doi.org/10.1016/S0009-2541(03)00207-9.

Lasaga, A.C. (1998) Kinetic Theory in the Earth Sciences, 811 p. Princeton University Press.

Li, M., Wang, L., Zhang, W., Putnis, C.V., and Putnis, A. (2016) Direct observation of spiral growth, particle attachment, and morphology evolution of hydroxyapatite. Crystal Growth & Design, 16, 4509–4518, https://doi.org/10.1021/acs.cgd.6b00637.

Mallin, M.A. and Cahoon, L.B. (2020) The hidden impacts of phosphorus pollution to streams and rivers. Bioscience, 70, 315–329, https://doi.org/10.1093/biosci/biaa001.

Mavropoulos, E., Rossi, A.M., Costa, A.M., Perez, C.A.C., Moreira, J.C., and Saldanha, M. (2002) Studies on the mechanisms of lead immobilization by hydroxyapatite. Environmental Science & Technology, 36, 1625–1629, https://doi.org/10.1021/es0155938.

McDowell, H., Gregory, T.M., and Brown, W.E. (1977) Solubility of $Ca_5(PO_4)_3OH$ in

the system $Ca(OH)_2$-$H_3PO_4$-$H_2O$ at 5, 15, 25, and 37 °C. Journal of Research of the National Bureau of Standards: Physics and Chemistry, 81A, 273–281, https://doi.org/10.6028/jres.081A.017.

Morales, J., Astilleros, J.M., Jiménez, A., Göttlicher, J., Steininger, R., and Fernández-Díaz, L. (2014) Uptake of dissolved lead by anhydrite surfaces. Applied Geochemistry, 40, 89–96, https://doi.org/10.1016/j.apgeochem.2013.11.002.

Murray, R.C. (1964) Origin and diagenesis of gypsum and anhydrite. Journal of Sedimentary Research, 34, 512–523.

Nakamura, S., Otsuka, R., Aoki, H., Akao, M., Miura, N., and Yamamoto, T. (1990) Thermal expansion of hydroxyapatite-β-tricalcium phosphate ceramics. Thermochimica Acta, 165, 57–72, https://doi.org/10.1016/0040-6031(90)80206-E.

Olivarius, M., Weibel, R., Hjuler, M.L., Kristensen, L., Mathiesen, A., Nielsen, L.H., and Kjøller, C. (2015) Diagenetic effects on porosity–permeability relationships in red beds of the Lower Triassic Bunter Sandstone Formation in the North German Basin. Sedimentary Geology, 321, 139–153, https://doi.org/10.1016/j.sedgeo.2015.03.003.

Otálora, F. and García-Ruiz, J. (2014) Nucleation and growth of the Naica giant gypsum crystals. Chemical Society Reviews, 43, 2013–2026, https://doi.org/10.1039/C3CS60320B.

Parkhurst, D.L. and Appelo, C. (1999) User's Guide to PHREEQC (ver. 2): A computer program for speciation, batch-reaction, one-dimensional transport, and inverse geochemical calculations. Water-resources Investigations Report, 99, 312.

Pedrosa, E.T., Putnis, C.V., and Putnis, A. (2016) The pseudomorphic replacement of marble by apatite: The role of fluid composition. Chemical Geology, 425, 1–11, https://doi.org/10.1016/j.chemgeo.2016.01.022.

Pedrosa, E.T., Boeck, L., Putnis, C.V., and Putnis, A. (2017) The replacement of a carbonate rock by fluorite: Kinetics and microstructure. American Mineralogist, 102, 126–134, https://doi.org/10.2138/am-2017-5725.

Penel, G., Leroy, G., Rey, C., and Bres, E. (1998) MicroRaman spectral study of the $PO_4$ and $CO_3$ vibrational modes in synthetic and biological apatites. Calcified Tissue International, 63, 475–481, https://doi.org/10.1007/s002239900561.

Pinto, A.J., Jimenez, A., and Prieto, M. (2009) Interaction of phosphate-bearing solutions with gypsum: Epitaxy and induced twinning of brushite ($CaHPO_4 \cdot 2H_2O$) on the gypsum cleavage surface. American Mineralogist, 94, 313–322, https://doi.org/10.2138/am.2009.3046.

Pinto, A.J., Carneiro, J., Katsikopoulos, D., Jiménez, A., and Prieto, M. (2012) The Link between Brushite and Gypsum: Miscibility, Dehydration, and Crystallochemical Behavior in the $CaHPO_4 \cdot 2H_2O$–$CaSO_4 \cdot 2H_2O$ System. Crystal Growth & Design, 12, 445–455, https://doi.org/10.1021/cg2012815.

Pollok, K., Putnis, C.V., and Putnis, A. (2011) Mineral replacement reactions in solid solution-aqueous solution systems: Volume changes, reactions paths and endpoints using the example of model salt systems. American Journal of Science, 311, 211–236, https://doi.org/10.2475/03.2011.02.

Putnis, A. (1992) An Introduction to Mineral Sciences, 480 p. Cambridge University Press.

——— (2002) Mineral replacement reactions: From macroscopic observations to microscopic mechanisms. Mineralogical Magazine, 66, 689–708, https://doi.org/10.1180/0026461026650056.

——— (2009) Mineral replacement reactions. Reviews in Mineralogy and Geochemistry, 70, 87–124, https://doi.org/10.2138/rmg.2009.70.3.

——— (2015) Transient porosity resulting from fluid-mineral interaction and its consequences. Reviews in Mineralogy and Geochemistry, 80, 1–23, https://doi.org/10.2138/rmg.2015.80.01.

Putnis, A. and Putnis, C.V. (2007) The mechanism of reequilibration of solids in the presence of a fluid phase. Journal of Solid State Chemistry, 180, 1783–1786, https://doi.org/10.1016/j.jssc.2007.03.023.

Putnis, C.V., Tsukamoto, K., and Nishimura, Y. (2005) Direct observations of pseudomorphism: Compositional and textural evolution at a fluid-solid interface. American Mineralogist, 90, 1909–1912, https://doi.org/10.2138/am.2005.1990.

Rahimpour-Bonab, H., Esrafili-Dizaji, B., and Tavakoli, V. (2010) Dolomitization and anhydrite precipitation in Permo-Triassic carbonates at the South Pars gas Field, Offshore Iran: Controls on reservoir quality. Journal of Petroleum Geology, 33, 43–66, https://doi.org/10.1111/j.1747-5457.2010.00463.x.

Rakovan, J. and Reeder, R.J. (1996) Intracrystalline rare earth element distributions in apatite: Surface structural influences on incorporation during growth. Geochimica et Cosmochimica Acta, 60, 4435–4445, https://doi.org/10.1016/S0016-7037(96)00244-X.

Redfern, S.A.T. (1987) The kinetics of dehydroxylation of kaolinite. Clay Minerals, 22, 447–456, https://doi.org/10.1180/claymin.1987.022.4.08.

Reinares-Fisac, D., Veintemillas-Verdaguer, S., and Fernández-Díaz, L. (2017) Conversion of biogenic aragonite into hydroxyapatite scaffolds in boiling solutions. CrystEngComm, 19, 110–116, https://doi.org/10.1039/C6CE01725H.

Rodríguez-Blanco, J.D., Jiménez, A., and Prieto, M. (2007) Oriented Overgrowth of Pharmacolite ($CaHAsO_4 \cdot 2H_2O$) on Gypsum ($CaSO_4 \cdot 2H_2O$). Crystal Growth & Design, 7, 2756–2763, https://doi.org/10.1021/cg070222+.

Roy, D.M. and Linnehan, S.K. (1974) Hydroxyapatite formed from coral skeletal carbonate by hydrothermal exchange. Nature, 247, 220–222, https://doi.org/10.1038/247220a0.

Roza Llera, A., Jimenez, A., and Fernández-Díaz, L. (2021) Removal of Pb from water: The effectiveness of gypsum and calcite mixtures. Minerals, 11, 66, https://doi.org/10.3390/min11010066.

Ruiz-Agudo, E., Putnis, C.V., and Putnis, A. (2014) Coupled dissolution and precipitation at mineral-fluid interfaces. Chemical Geology, 383, 132–146, https://doi.org/10.1016/j.chemgeo.2014.06.007.

Ruiz-Agudo, E., Putnis, C.V., Hövelmann, J., Álvarez-Lloret, P., Ibañez-Velasco, A., and Putnis, A. (2015) Experimental study of the replacement of calcite by calcium sulphates. Geochimica et Cosmochimica Acta, 156, 75–93, https://doi.org/10.1016/j.gca.2015.02.012.

Sheldon, R.P. (1981) Ancient marine phosphorites. Annual Review of Earth and Planetary Sciences, 9, 251–284, https://doi.org/10.1146/annurev.ea.09.050181.001343.

Smith, V.H. (2003) Eutrophication of freshwater and coastal marine ecosystems: A global problem. Environmental Science and Pollution Research International, 10, 126–139, https://doi.org/10.1065/espr2002.12.142.

Wang, L. and Nancollas, G.H. (2008) Calcium orthophosphates: Crystallization and dissolution. Chemical Reviews, 108, 4628–4669, https://doi.org/10.1021/cr0782574.

Wang, L., Ruiz-Agudo, E., Putnis, C.V., Menneken, M., and Putnis, A. (2012) Kinetics of calcium phosphate nucleation and growth on calcite: Implications for predicting the fate of dissolved phosphate species in alkaline soils. Environmental Science & Technology, 46, 834–842, https://doi.org/10.1021/es202924f.

Wang, L., Putnis, C.V., Ruiz-Agudo, E., Hövelmann, J., and Putnis, A. (2015) In situ imaging of interfacial precipitation of phosphate on Goethite. Environmental Science & Technology, 49, 4184–4192, https://doi.org/10.1021/acs.est.5b00312.

Wei, X. and Bailey, R.T. (2021) Evaluating nitrate and phosphorus remediation in intensively irrigated stream-aquifer systems using a coupled flow and reactive transport model. Journal of Hydrology (Amsterdam), 598, 126304, https://doi.org/10.1016/j.jhydrol.2021.126304.

Xia, F., Brugger, J., Chen, G., Ngothai, Y., O'Neill, B., Putnis, A., and Pring, A. (2009) Mechanism and kinetics of pseudomorphic mineral replacement reactions: A case study of the replacement of pentlandite by violarite. Geochimica et Cosmochimica Acta, 73, 1945–1969, https://doi.org/10.1016/j.gca.2009.01.007.

Yang, Y., Wu, Q., Wang, M., Long, J., Mao, Z., and Chen, X. (2014) Hydrothermal synthesis of hydroxyapatite with different morphologies: Influence of supersaturation of the reaction system. Crystal Growth & Design, 14, 4864–4871, https://doi.org/10.1021/cg501063j.

Yuan, K., De Andrade, V., Feng, Z., Sturchio, N.C., Lee, S.S., and Fenter, P. (2018) $Pb^{2+}$-calcite interactions under far-from-equilibrium conditions: Formation of Micropyramids and pseudomorphic growth of cerussite. The Journal of Physical Chemistry C, 122, 2238–2247, https://doi.org/10.1021/acs.jpcc.7b11682.

Zhao, J., Brugger, J., Grundler, P.V., Xia, F., Chen, G., and Pring, A. (2009) Mechanism and kinetics of a mineral transformation under hydrothermal conditions: Calaverite to metallic gold. American Mineralogist, 94, 1541–1555, https://doi.org/10.2138/am.2009.3252.

Zhu, R., Yu, R., Yao, J., Wang, D., and Ke, J. (2008) Morphology control of hydroxyapatite through hydrothermal process. Journal of Alloys and Compounds, 457, 555–559, https://doi.org/10.1016/j.jallcom.2007.03.081.

Manuscript received May 13, 2022
Manuscript accepted October 13, 2022
Accepted manuscript online October 27, 2022
Manuscript handled by Jie Xu

## Endnote:

[1]Deposit item AM-23-98592. Online Materials are free to all readers. Go online, via the table of contents or article view, and find the tab or link for supplemental materials.